Current Biology 22, 2081–2085, November 6, 2012 ©2012 Elsevier Ltd All rights reserved http://dx.doi.org/10.1016/j.cub.2012.09.014

Report

The Retinotopic Organization of Striate Cortex Is Well Predicted by Surface Topology

Noah C. Benson,[1,2,3] Omar H. Butt,[1,3] Ritobrato Datta,[1] Petya D. Radoeva,[1] David H. Brainard,[2] and Geoffrey K. Aguirre[1,*]
[1]Department of Neurology
[2]Department of Psychology
University of Pennsylvania, Philadelphia, PA 19104, USA

Summary

In 1918, Gordon Holmes combined observations of visual-field scotomas across brain-lesioned soldiers to produce a schematic map of the projection of the visual field upon the striate cortex [1]. One limit to the precision of his result, and the mapping of anatomy to retinotopy generally, is the substantial individual variation in the size [2, 3], volumetric position [4], and cortical magnification [5] of area V1. When viewed within the context of the curvature of the cortical surface, however, the boundaries of striate cortex fall at a consistent location across individuals [6]. We asked whether the surface topology of the human brain can be used to accurately predict the internal, retinotopic function of striate cortex as well. We used fMRI to measure polar angle and eccentricity in 25 participants and combined their maps within a left-right, transform-symmetric representation of the cortical surface [7]. These data were then fit using a deterministic, algebraic model of visual-field representation [8]. We found that an anatomical image alone can be used to predict the retinotopic organization of striate cortex for an individual with accuracy equivalent to 10–25 min of functional mapping. This indicates tight developmental linkage of structure and function within a primary, sensory cortical area.

Results

We obtained retinotopic mapping (RM) data for the central 10° of visual field from 19 participants and the central 20° from a separate group of 6 participants. Voxelwise polar angle and eccentricity were determined using population receptive field (pRF) methods [9]. Spatially unsmoothed data were combined across hemispheres and subjects within a left-right symmetric, spherical atlas of sulcal topology [7, 10]. Figure 1A illustrates the transformation of polar angle data from the initial pial representation for one subject to the template cortical sphere. Analyses of retinotopic organization were conducted within a region predicted by cortical topology to contain striate cortex [6] (Figure 1B). We developed an automatic and deterministic algorithm for fitting a retinotopic model to anatomically defined area V1 in the absence of user input (see Experimental Procedures). We then asked whether the RM data from a group could be used to predict the RM of an individual given only an anatomical brain image.

Anatomical Prediction of Polar Angle

Representation of polar angle has been found to correspond to the gyral and sulcal curvature of the cortical surface [11]. When aligned using sulcal topology as a guide, the average polar angle representation across subjects from the 10° data set (Figure 2A) demonstrates this relationship and confirms the accuracy of the anatomically defined borders of V1 [6]. At the posterior extent of V1, the measured polar angle representation becomes disorganized as multiple lines of azimuth intersect within the foveal confluence [12].

The aggregate polar angle data were compared to an algebraic template fit to the polar angle data of all subjects in the 10° data set (Figure 2B; see Supplemental Information for details). This template performed nearly uniformly over the extent of V1 for which retinotopic mapping data were available (Figure 2C).

We next asked how well the retinotopic template generated using our procedure could predict the measured polar angle for an individual. For each subject, a template to which they were compared was constructed using data from all other subjects in a leave-one-out fashion. This template was then used to predict the spatially unsmoothed polar angle organization of the excluded subject, guided only by that subject's cortical anatomy. Figure 2D shows the median absolute error across subjects for the prediction of polar angle along isoangular bands defined by the template. The median absolute error in the prediction of polar angle was below 12° when aggregated across subjects in a leave-one-out fashion (median absolute and signed errors across all vertices in V1 were 11.43° and −0.93°, respectively, for leave-one-out comparisons).

Finally, we confirmed that the polar angle fits derived from one group of subjects generalized to a second group. The polar angle fit to the aggregate of data from the 10° data set (Figure 2E) matched the fit to the aggregate data from subjects in the 20° data set (Figure 2F).

Anatomical Prediction of Eccentricity

The unsmoothed eccentricity measurements from 19 subjects, studied with RM stimulation out to 10°, were combined (Figure 3A). An area of low-eccentricity values can be seen extending posteriorly beyond the predicted border of area V1, corresponding to the foveal confluence.

The aggregate eccentricity data were fit with an exponential template (Figure 3B). Only those points with an assigned eccentricity below 8° and above 2.5° informed the fit, to avoid a bias in the measurement of eccentricity that occurs near the border of the mapping stimulus [13] and near the foveal confluence. The residuals of the fit to the aggregate data (Figure 3C) show increasing error as the template approaches 10° of eccentricity; below, we demonstrate that bias in the empirical measurement of eccentricity is responsible for this deviation.

A leave-one-out analysis tested whether unsmoothed retinotopic eccentricity could be predicted for individual subjects from their anatomy (Figure 3D). The error across subjects in specification of retinotopic eccentricity from anatomy is generally <1.0° but, as with the aggregate residual error (Figure 3C), increases sharply beyond approximately 8°

[3]These authors contributed equally to this work
*Correspondence: aguirreg@mail.med.upenn.edu

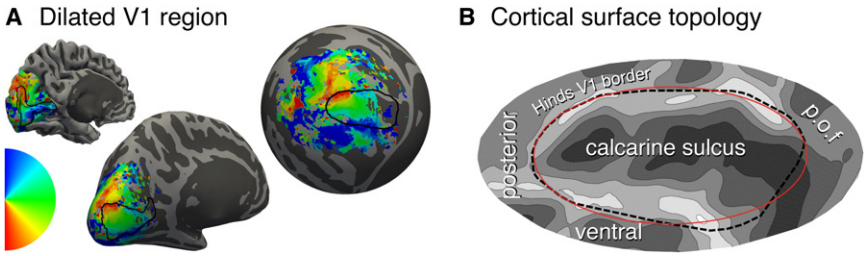

Figure 1. Cortical Surface Atlas Space

(A) Polar angle assignment is plotted on the folded (left), inflated (center), and spherical (right) hemisphere of a single subject. The black line shows the Hinds et al. [6] V1 outline.

(B) Cortical folding and landmarks around area V1. The calcarine sulcus and parieto-occipital fissure (p.o.f.) are indicated. The red ellipse defines the border of the algebraic template. Figure S1 illustrates the projection of the visual field onto this patch of cortex.

of template eccentricity (the median absolute and signed leave-one-out errors for all vertices in V1 with template values between 2.5° and 8° were 0.91° and 0.39°).

If measurement bias near the edge of the stimulus is responsible for the apparent template inaccuracy between 8° and 10° eccentricity, then the performance of the template in this range should be restored for data collected with more eccentric stimulation. We fit our model to the aggregate of subjects studied with a stimulus that extended to 20°, again excluding those points within 2° of the outer edge of the stimulus. We asked how well the cortical eccentricity function derived from these data would match that measured using the inner 8° of the 10° data set. Figure 3E is a histogram of every vertex from every subject from the 10° study; Figure 3F plots all vertices from the 20° study. We find that the exponential cortical eccentricity functions fit to the two independent data sets are almost perfectly superimposed and that the spread of points seen near the stimulus border of the 10° data set (Figure 3E) has condensed. Therefore, not only can cortical anatomy predict eccentricity organization with a median absolute error of <1°, it is more accurate than measurement itself near the stimulus border.

Measurement Error

A limit on the accuracy of template prediction is error in the measurement of visual-field values for individual subjects. We examined the within-subject, median split-halves measurement error of eccentricity in the 10° data set (Figure 4) and found that it is only modestly lower (0.75°) than the median leave-one-out error of the anatomical template (0.91°). This comparison suggests that a substantial proportion of the residual error of the template can be attributed to measurement error in individual subjects; this error would persist even in the presence of a perfect template representation. The corresponding split-half analysis of polar angle (Figures S3A and S3B) yielded similar results, with a median absolute

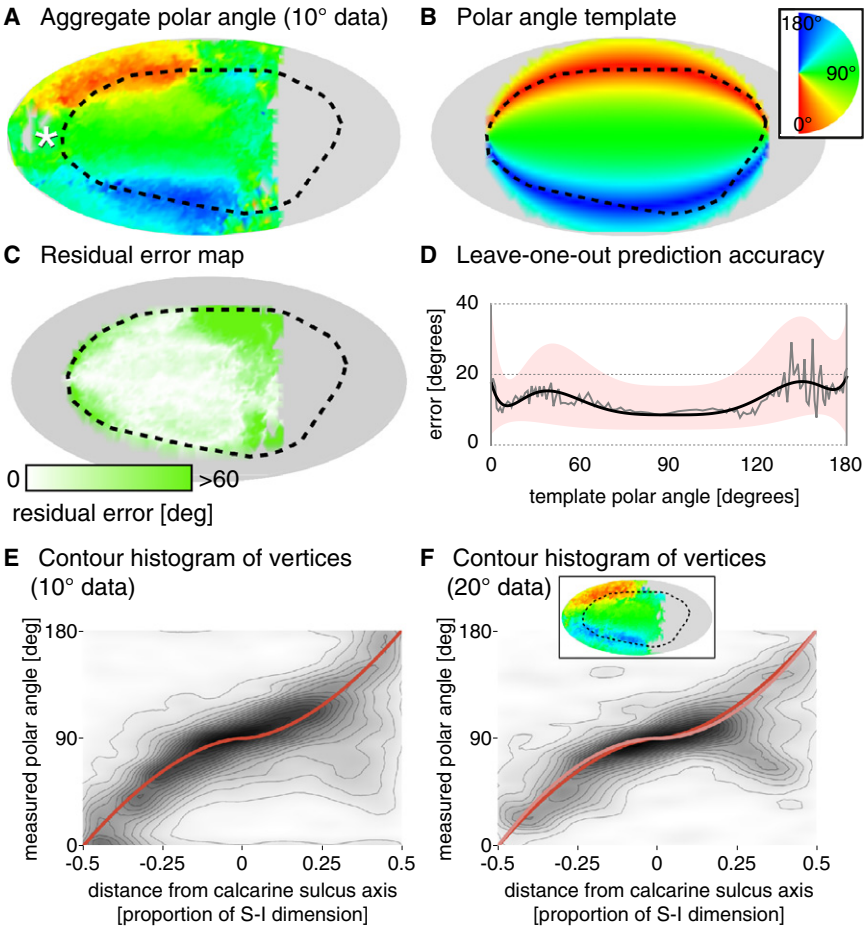

Figure 2. Polar Angle Prediction

(A) Aggregate polar angle data of 18 of the 19 subjects shown visual stimuli within 10° of fixation (one significant outlier excluded). White asterisk is the foveal confluence; black dashed line is the Hinds et al. [6] V1 border.

(B) Algebraic template, fit to the aggregate polar angle map.

(C) Absolute residual error between the template fit and aggregate data.

(D) Median absolute prediction error across vertices and subjects by template polar angle. The median error (gray) is fit by a fifth-order polynomial (black) with the similarly fit upper and lower quartiles defining the border of the pink region.

(E) Contour histogram of all vertices from 10° data set subjects, binned by measured polar angle and superior-inferior position in the template space. The template fit is shown in red. Each contour line corresponds to ~2,000 vertices.

(F) Corresponding contour histogram from 20° data set subjects. The template fit to the 20° data set is in pink, and the fit to the 10° data set is reproduced from (E) in red. Each contour line corresponds to ~700 vertices. Inset is the aggregate map for the 20° data set. Figure S2A presents the polar angle aggregates and fits by hemisphere, and Table S1 provides the exact formula measurements.

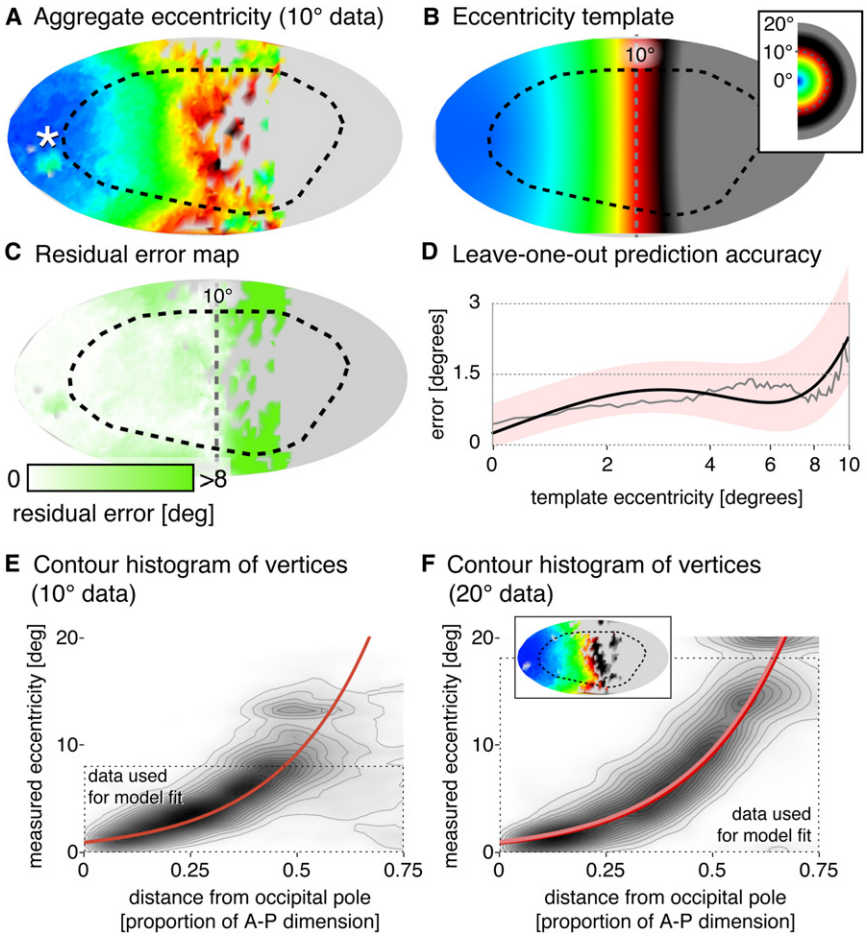

Figure 3. Eccentricity Prediction

(A) Aggregate eccentricity data of subjects (n = 19) shown visual stimuli within 10° of fixation. White asterisk is the foveal confluence; black dashed line is the Hinds et al. [6] V1 border.

(B) Algebraic model, fit to the aggregate eccentricity map, after excluding those points with values $\leq 2.5°$ and $\geq 8°$.

(C) Absolute residual error between the template fit and aggregate data.

(D) Median absolute prediction error across vertices and subjects by template eccentricity. The median error (gray) is fit by a fifth-order polynomial (black) with the similarly fit upper and lower quartiles defining the border of the pink region.

(E) Contour histogram of all vertices from 10° data set subjects, binned by measured eccentricity and posterior-anterior position in the template space. The exponential template fit is shown in red. Each contour line corresponds to ~2,000 vertices.

(F) Corresponding contour histogram from 20° data set subjects. The template fit to the 20° data set is in pink, and the fit to the 10° data set is reproduced from (E) in red. Each contour line corresponds to ~800 vertices. Inset is the aggregate map for the 20° data set. Figure S2B presents the eccentricity prediction aggregates and fits by hemisphere, and Table S1 provides the exact formula measurements.

error of 7.76°, compared to the template's leave-one-out error of 11.43°. The Supplemental Information considers other sources of variability, including anatomical registration and hemispheric differences (Figure S2; Table S1).

To estimate the scan time needed to obtain retinotopic mapping with the same median absolute error as that of anatomical prediction, we collected 96 min of RM data for a single example subject (a 22-year-old male with normal vision). Forty-eight minutes of data were compared to disjoint 16, 32, and 48 min subsets of the scan, and the median absolute error of each comparison was fit with a decaying exponential (Figures S3D and S3E). We found that ~25 min of retinotopic mapping data in this (arguably optimal) participant was needed to match the prediction performance of our template for polar angle in the other 19 subjects, and ~10 min of scanning was needed to match the template eccentricity performance.

Discussion

Topographic maps are a common motif in the cortical organization of sensory information. Such maps have been observed in the tonotopic mapping of the primary auditory cortex [14–16] and the somatotopic mapping of the sensorimotor cortex [17–19]. A fundamental question is whether these maps develop in a systematic manner with respect to cortical structure. In the case of sensorimotor cortex, for example, a characteristic "knob" on the precentral gyrus is associated with the motor representation of the hand [20]. For the primary visual cortex, prior work has established that the calcarine sulcus represents the horizontal azimuth [11]. We extend this finding here by demonstrating that the polar angle and eccentricity representation of the visual world are tightly coupled to sulcal folding anatomy.

This regularity is captured within an algebraic template of the retinotopic map. The template fitting procedure is automatic, nonstochastic, and independent of user choices such as anatomical landmarks. These features allow the ready comparison of retinotopy from individuals or populations while avoiding sources of human error.

The automated fit to V1 may also serve as a starting point for template fitting of higher-order visual areas. The Schira et al. model [8], upon which we based our template, extends lines of eccentricity and polar angle to surrounding visual areas, providing a ready mechanism for template extension. Another useful target is the foveal confluence, which is challenging to define by RM methods. Notably, data collected with higher spatial resolution [12] could be used to further refine our template within this region. The success of these extensions is both dependent upon and informative regarding the presence of subject variability in structure-function mapping beyond primary visual cortex. Examination of cytoarchitecture in cadaveric brains within an automated surface template has shown that higher-order cortical areas (e.g., V2, Broca's area) are more variable in location than primary areas such as V1 or primary somatosensory cortex [21]. Further improvements in anatomical registration may resolve this variability, although the automated software used here (FreeSurfer) already has accuracy comparable to human-guided, landmark-based

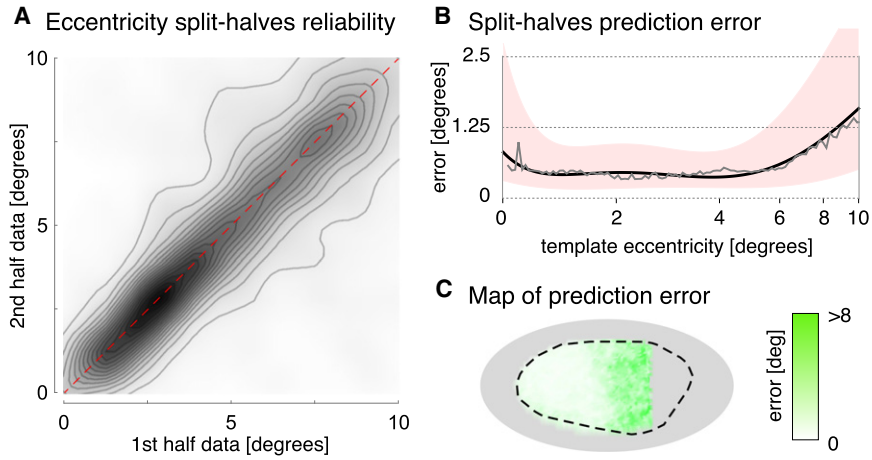

Figure 4. Split-Halves Reliability of Eccentricity

(A) A split-halves analysis plotted the eccentricity measured for each vertex for each subject from the first half of each ~30 min scan against the eccentricity derived from the same vertex during the second half-scan. Each contour line corresponds to ~4,100 vertices.

(B) Median absolute split-halves error across vertices and subjects by template eccentricity. The median error (gray) is fit by a fifth-order polynomial (black) with the similarly fit upper and lower quartiles defining the border of the pink region.

(C) Test-retest absolute residuals between first- and second-half measurements for each vertex shown on the cortical surface. Figure S3 presents the corresponding measurements for polar angle.

alignment for the calcarine sulcus [22]. Alternatively, the extent of striate cortex may be defined by direct imaging of intracortical myelination [23], providing a still firmer basis for initial, between-subject alignment of area V1.

Practically, we have found that anatomical imaging alone can predict retinotopic arrangement with a precision comparable to 10–25 min of fMRI. The relative performance of anatomical prediction is doubtless better in populations less able to cooperate with maintaining the attention, gaze fixation, and head immobility required for functional mapping studies. Patients with ophthalmologic disease are an obvious target for the use of anatomically derived retinotopic maps.

Finally, our work may be regarded as the culmination of an enterprise started by Gordon Holmes in 1918, when he provided a map of the "cortical retina" by relating perimetric visual-field scotomas to the trajectory of missile wounds to the brain [1]. The final diagram of his report offers a "probable representation of the different portions of the visual fields in the calcarine cortex." In the legend below this figure—remarkable for its timelessness, given the crude technique he had available—Holmes cautions that "this diagram does not claim to be in any respect accurate; it is merely a schema." The atlas we have produced is a descendent of Holmes's effort for which we can claim accuracy, and with known precision.

Experimental Procedures

Subjects and Stimuli

Twenty-five subjects (15 women, 10 men; mean age 24 years, age range 20–42 years) with normal vision participated in fMRI scanning experiments. The study was approved by the University of Pennsylvania Institutional Review Board, and all subjects provided written informed consent.

Two primary data sets were collected. The first, 10° data set (19 subjects) used a single sweeping bar of 2.5° thickness that flickered at 5 Hz [9]. The bar traveled 1.25° every 3 s within a central 20° aperture in four orientations (horizontal, vertical, oblique +45°, oblique −45°) over 27 min while subjects maintained central fixation. For the second, 20° data set, six subjects were studied while they maintained fixation on the left or right side of the screen while standard "ring and wedge" stimuli [24] swept in the periphery in 16 steps. Sixty-four minutes of data were obtained during stimulation of each visual field.

Magnetic Resonance Imaging

Whole-brain blood oxygen level-dependent (BOLD) fMRI data (repetition time 3 s, 3 mm isotropic voxels) and a standard T1-weighted anatomical image (1 mm isotropic voxels) were acquired at 3 T. Anatomical data were processed using the FMRIB Software Library (FSL) toolkit (http://fsl.fmrib.ox.ac.uk/fsl/) and individual subject brain surfaces reconstructed and inflated using FreeSurfer (v5.1) (http://surfer.nmr.mgh.harvard.edu/) [10, 25, 26]. Individual hemispheric maps were registered to a common FreeSurfer template surface pseudohemisphere (fsaverage_sym; http://surfer.nmr.mgh.harvard.edu/fswiki/Xhemi) [7, 21]. Probabilistic boundaries for V1 in the reconstructed brain surface for each subject were generated using atlas definitions [6].

Calculation of Retinotopic Mapping Values

Initial statistical analysis used a finite impulse response (FIR) basis of shifted delta functions to model neural response to the stimulus positions. The BOLD signal was modeled with a population average hemodynamic response (HRF) [27] (for the 10° data set) or with a subject-specific HRF derived from a separate, blocked visual stimulation scan (for the 20° data set). Nuisance covariates included effects of scan, global signals, spikes (periods of raw signal deviation greater than two standard deviations from the mean), and cardiac and respiratory fluctuations from simultaneously recorded pulse oximetry (when available) [28]. Polar angle and eccentricity values were defined either by the population receptive field (pRF) approach [9] (for the 10° data set) or by identification of the peak of a Gaussian fit to the set of FIR β weights derived from the initial linear model analysis (for the 20° data set).

Data Aggregation and Template Fitting

Vertices from the predicted V1 region [6] were projected from 3D surface coordinates to a 2D map with a shear transformation applied to reduce spherical curvature in the embedding. Aggregate maps were constructed by taking the mean polar angle or eccentricity for each vertex position across all subjects with responses at that position. Vertices for which two or fewer subjects had significant BOLD responses or for which the standard deviation of responses was greater than 3.3° of eccentricity or 60° of polar angle were excluded from the aggregate fits due to low confidence.

An algebraic model was fit to the aggregate RM data within the 2D space. The boundaries of V1 were defined by an ellipse. Isoeccentric bands within V1 followed hyperbolas that were orthogonal to the isoangular bands, which were also ellipses (see Supplemental Experimental Procedures and Figure S1).

For fitting of the eccentricity model, all vertices whose eccentricity values were within 2° of the outer stimulus border were discarded to avoid previously described measurement bias at the stimulus edges [13], as were voxels whose responses were <2.5°.

Fitting was performed using a nonlinear numeric log error minimization technique on the spatially unsmoothed retinotopic data. For eccentricity, the template was exponential along isoangular bands (i.e., eccentricity varied exponentially across isoangular bands) using published starting parameters [5]. The template was given the form $r = 90^{\circ}\exp(q(x-1))$, where x is the coordinate of the isoeccentric band passing through a particular point and q is the fit parameter. For polar angle, the template was polynomial with a starting parameter of 1. The template was given the form $\theta = 90^{\circ} + 90^{\circ}\ \mathrm{sgn}(y)\ |y|^{q}$, where y is the coordinate of the isoangular band passing through a particular point and q is the fit parameter.

Additional data and templates are available from https://cfn.upenn.edu/aguirre/wiki/public:data_currbio_2012_benson.

Supplemental Information

Supplemental Information includes three figures, one table, Supplemental Experimental Procedures, and a Mathematica notebook and can be found with this article online at http://dx.doi.org/10.1016/j.cub.2012.09.014.

Acknowledgments

We thank G. Boynton for his thoughts regarding bias in measurement of eccentricity and C. Broussard for developing the visual stimulation software. This work was supported by a Pennsylvania State CURE grant and NIH grants P30 EY001583, P30 NS045839-08, and 1 R01 EY020516-01A1.

Received: January 25, 2012
Revised: July 24, 2012
Accepted: September 7, 2012
Published online: October 4, 2012

References

1. Holmes, G. (1918). Disturbances of vision by cerebral lesions. Br. J. Ophthalmol. *2*, 353–384.
2. Andrews, T.J., Halpern, S.D., and Purves, D. (1997). Correlated size variations in human visual cortex, lateral geniculate nucleus, and optic tract. J. Neurosci. *17*, 2859–2868.
3. Dougherty, R.F., Koch, V.M., Brewer, A.A., Fischer, B., Modersitzki, J., and Wandell, B.A. (2003). Visual field representations and locations of visual areas V1/2/3 in human visual cortex. J. Vis. *3*, 586–598.
4. Amunts, K., Malikovic, A., Mohlberg, H., Schormann, T., and Zilles, K. (2000). Brodmann's areas 17 and 18 brought into stereotaxic space-where and how variable? Neuroimage *11*, 66–84.
5. Qiu, A., Rosenau, B.J., Greenberg, A.S., Hurdal, M.K., Barta, P., Yantis, S., and Miller, M.I. (2006). Estimating linear cortical magnification in human primary visual cortex via dynamic programming. Neuroimage *31*, 125–138.
6. Hinds, O.P., Rajendran, N., Polimeni, J.R., Augustinack, J.C., Wiggins, G., Wald, L.L., Diana Rosas, H., Potthast, A., Schwartz, E.L., and Fischl, B. (2008). Accurate prediction of V1 location from cortical folds in a surface coordinate system. Neuroimage *39*, 1585–1599.
7. Greve, D.N., Sabuncu, M.R., Shafee, R., Schmansky, N., Buckner, R.L., and Fischl, B. (2011). Automatic surface-based interhemispheric registration with FreeSurfer (Quebec City, Canada: 17th Annual Meeting of the Organization on Human Brain Mapping, June 26–30, 2011). http://www.nmr.mgh.harvard.edu/martinos/publications/posters/HBM-2011/HBM11-Greve.pdf.
8. Schira, M.M., Tyler, C.W., Spehar, B., and Breakspear, M. (2010). Modeling magnification and anisotropy in the primate foveal confluence. PLoS Comput. Biol. *6*, e1000651.
9. Dumoulin, S.O., and Wandell, B.A. (2008). Population receptive field estimates in human visual cortex. Neuroimage *39*, 647–660.
10. Fischl, B., and Dale, A.M. (2000). Measuring the thickness of the human cerebral cortex from magnetic resonance images. Proc. Natl. Acad. Sci. USA *97*, 11050–11055.
11. Rajimehr, R., and Tootell, R.B.H. (2009). Does retinotopy influence cortical folding in primate visual cortex? J. Neurosci. *29*, 11149–11152.
12. Schira, M.M., Tyler, C.W., Breakspear, M., and Spehar, B. (2009). The foveal confluence in human visual cortex. J. Neurosci. *29*, 9050–9058.
13. Baseler, H.A., Brewer, A.A., Sharpe, L.T., Morland, A.B., Jägle, H., and Wandell, B.A. (2002). Reorganization of human cortical maps caused by inherited photoreceptor abnormalities. Nat. Neurosci. *5*, 364–370.
14. Formisano, E., Kim, D.S., Di Salle, F., van de Moortele, P.F., Ugurbil, K., and Goebel, R. (2003). Mirror-symmetric tonotopic maps in human primary auditory cortex. Neuron *40*, 859–869.
15. Humphries, C., Liebenthal, E., and Binder, J.R. (2010). Tonotopic organization of human auditory cortex. Neuroimage *50*, 1202–1211.
16. Striem-Amit, E., Hertz, U., and Amedi, A. (2011). Extensive cochleotopic mapping of human auditory cortical fields obtained with phase-encoding FMRI. PLoS ONE *6*, e17832.
17. Penfield, W., and Boldrey, E. (1937). Somatic motor and sensory representation in the cerebral cortex of man as studied by electrical stimulation. Brain *60*, 389–443.
18. Grafton, S.T., Woods, R.P., Mazziotta, J.C., and Phelps, M.E. (1991). Somatotopic mapping of the primary motor cortex in humans: activation studies with cerebral blood flow and positron emission tomography. J. Neurophysiol. *66*, 735–743.
19. Rao, S.M., Binder, J.R., Hammeke, T.A., Bandettini, P.A., Bobholz, J.A., Frost, J.A., Myklebust, B.M., Jacobson, R.D., and Hyde, J.S. (1995). Somatotopic mapping of the human primary motor cortex with functional magnetic resonance imaging. Neurology *45*, 919–924.
20. Yousry, T.A., Schmid, U.D., Alkadhi, H., Schmidt, D., Peraud, A., Buettner, A., and Winkler, P. (1997). Localization of the motor hand area to a knob on the precentral gyrus. A new landmark. Brain *120*, 141–157.
21. Fischl, B., Sereno, M.I., Tootell, R.B., and Dale, A.M. (1999). High-resolution intersubject averaging and a coordinate system for the cortical surface. Hum. Brain Mapp. *8*, 272–284.
22. Pantazis, D., Joshi, A., Jiang, J., Shattuck, D.W., Bernstein, L.E., Damasio, H., and Leahy, R.M. (2010). Comparison of landmark-based and automatic methods for cortical surface registration. Neuroimage *49*, 2479–2493.
23. Trampel, R., Ott, D.V., and Turner, R. (2011). Do the congenitally blind have a stria of Gennari? First intracortical insights in vivo. Cereb. Cortex *21*, 2075–2081.
24. Engel, S.A., Glover, G.H., and Wandell, B.A. (1997). Retinotopic organization in human visual cortex and the spatial precision of functional MRI. Cereb. Cortex *7*, 181–192.
25. Dale, A.M., Fischl, B., and Sereno, M.I. (1999). Cortical surface-based analysis. I. Segmentation and surface reconstruction. Neuroimage *9*, 179–194.
26. Salat, D.H., Buckner, R.L., Snyder, A.Z., Greve, D.N., Desikan, R.S., Busa, E., Morris, J.C., Dale, A.M., and Fischl, B. (2004). Thinning of the cerebral cortex in aging. Cereb. Cortex *14*, 721–730.
27. Aguirre, G.K., Zarahn, E., and D'esposito, M. (1998). The variability of human, BOLD hemodynamic responses. Neuroimage *8*, 360–369.
28. Verstynen, T.D., and Deshpande, V. (2011). Using pulse oximetry to account for high and low frequency physiological artifacts in the BOLD signal. Neuroimage *55*, 1633–1644, 30.